

Heat capacity measurements on FeAs-based compounds: a thermodynamic probe of electronic and magnetic states

P J Baker^{1,5}, S R Giblin², F L Pratt², R H Liu³, G Wu³,
X H Chen³, M J Pitcher⁴, D R Parker⁴, S J Clarke⁴
and S J Blundell¹

¹ Clarendon Laboratory, Department of Physics, University of Oxford,
Parks Road, Oxford, OX1 3PU, UK

² ISIS Muon Facility, Rutherford Appleton Laboratory, Harwell Science and
Innovation Campus, Didcot, OX11 0QX, UK

³ Hefei National Laboratory for Physical Sciences at Microscale and
Department of Physics, University of Science and Technology of China,
Hefei, Anhui 230026, People's Republic of China

⁴ Inorganic Chemistry Laboratory, Department of Chemistry,
University of Oxford, South Parks Road, Oxford, OX1 3QR, UK

E-mail: p.baker1@physics.ox.ac.uk

New Journal of Physics **11** (2009) 025010 (12pp)

Received 11 November 2008

Published 27 February 2009

Online at <http://www.njp.org/>

doi:10.1088/1367-2630/11/2/025010

Abstract. We report heat capacity measurements of the pnictide materials SmFeAsO_{1-x}F_x, NdFeAsO, LaFeAsO_{1-x}F_x and LiFeAs. For SmFeAsO_{1-x}F_x, with x close to 0.1, we use ³He measurements to demonstrate a transfer of entropy from the peak at T_N to a previously unidentified ~ 2 K feature, which grows with increasing doping. Our results on the Sm samples are compared with a similarly doped La sample to elucidate the crystal field levels of the Sm³⁺ ion at 0, 20 and 45 meV, which lead to a Schottky-like anomaly, and also show that there is a significant increase in the Sommerfeld coefficient γ when La is replaced by Sm or Nd. The lattice contribution to the heat capacity of the superconducting oxypnictides is found to vary negligibly with chemical substitution. We also present a heat capacity measurement of LiFeAs showing the feature at T_c , which is significantly rounded and much smaller than the BCS value.

⁵ Author to whom any correspondence should be addressed.

Contents

1. Introduction	2
2. Previous heat capacity studies of pnictide compounds	3
3. Experimental details	3
4. ^4He results on oxypnictides	4
5. ^3He results on oxypnictides	8
6. LiFeAs	9
7. Discussion	10
8. Conclusions	11
Acknowledgments	11
References	12

1. Introduction

The discovery of superconductivity in pnictide compounds containing iron came as an enormous surprise to the condensed matter physics and materials chemistry community. This started with derivatives of LaFePO ($T_c = 4\text{ K}$) [1], and then, attracting far greater attention, $\text{LaFeAsO}_{1-x}\text{F}_x$ ($T_c = 26\text{ K}$) [2]. The $\text{LnFeAsO}_{1-x}\text{F}_x$ (1111) materials have provided a remarkable range of superconducting materials with T_c rising quickly to 43 K in $\text{SmFeAsO}_{1-x}\text{F}_x$ [3], and subsequently to 55 K in that compound and oxygen-deficient $\text{SmFeAsO}_{1-\delta}$ [4, 5]. FeAs-based (122) materials with the general formula AFe_2As_2 ($T_c = 38\text{ K}$) [6, 7] and (111) materials such as LiFeAs ($T_c \sim 16\text{ K}$) [8, 9] and NaFeAs ($T_c = 9\text{ K}$) [10] also superconduct.

These new materials can be considered analogous to the cuprate high- T_c superconductors, but based on anti-PbO-type FeAs layers rather than planar CuO_2 layers. However, while the structural phase transitions occurring in the antiferromagnetic parent materials follow a similar pattern to those in the cuprates, the electronic and magnetic properties are significantly different: in cuprates, the parent materials are Mott insulators with localized moments, whereas pnictide parent materials are metallic and the magnetic moments are itinerant. Also, whereas one band models are effective in cuprates, five bands seem to be relevant to the superconductivity in pnictides. The superconducting properties and novel magnetism in these compounds have been a great spur to recent research. The tantalizing prospect is that the analogy will offer insights that will identify common aspects of the superconducting mechanism in both types of material. Specific heat measurements are powerful probes of magnetism and superconductivity since they probe the entropy involved with the electronic phase transitions and provide a straightforward comparison with theoretical work. In the pnictide superconductors, both Fe magnetism and superconductivity and the magnetic behaviour of the rare-earth moments are amenable to investigation using this technique.

In this paper, we present heat capacity results on three $\text{SmFeAsO}_{1-x}\text{F}_x$ samples in the doping range where the coexistence of magnetic order and superconductivity has been suggested, undoped SmFeAsO and NdFeAsO where magnetism is present without superconductivity and superconducting samples of $\text{LaFeAsO}_{1-x}\text{F}_x$ and LiFeAs where there is no magnetic order. Following a review of previous work (section 2) and a description of the technique (section 3), we present our results. These are divided into ^4He heat capacity results

on the oxypnictide compounds investigating the rare-earth magnetic order and excitations, iron moment ordering and superconductivity in section 4 and ^3He heat capacity results re-examining the rare-earth magnetic ordering in the same materials in section 5. The results on LiFeAs are presented in section 6. We discuss our findings in section 7.

2. Previous heat capacity studies of pnictide compounds

A significant number of specific heat measurements have already been carried out on pnictide compounds although they have covered only a small selection of the compounds synthesized so far. $\text{SmFeAsO}_{1-x}\text{F}_x$ has already been studied at the dopings $x = 0, 0.05, 0.15$ and 0.20 [11], and $0, 0.07$ and 0.15 [12], away from the intermediate doping range we consider here, revealing a peak in the specific heat in the undoped sample at $T_{\text{N}}^{\text{Fe}} \sim 130$ K and λ anomalies near $T_{\text{N}}^{\text{Sm}} \sim 4$ K.⁶ In $\text{LaFeAs}(\text{O},\text{F})$ [14, 15, 17], the structural (155 K) and magnetic transitions (143 K) are clearly resolved and have a small combined entropy of $0.032R$ [15]. The Sommerfeld coefficient was found to be relatively small, $\gamma = 3.7 \text{ mJ mol}^{-1} \text{ K}^{-2}$ [15]. The low-temperature values of γ were found to vary in applied magnetic field as $\gamma(H) \propto \sqrt{H}$, suggestive of line nodes in the superconducting gap function [17]. In this issue, McGuire *et al* [16] examined the structural and magnetic transitions around 150 K in CeFeAsO , PrFeAsO and NdFeAsO , finding clear separation between them and distinct heat capacity anomalies at each transition. LaFePO has also been studied in detail [18]–[20], $\gamma \sim 10 \text{ mJ mol}^{-1} \text{ K}^{-2}$ and relatively small specific heat jumps have been measured at T_{c} , $\Delta C_{\text{p}}/\gamma T_{\text{c}} \sim 0.6$.

A smaller number of 122 materials have also been measured: BaNi_2As_2 has a first-order phase transition at $T_0 = 130$ K and a Sommerfeld coefficient $\gamma = 10.8 \pm 0.1 \text{ mJ mol}^{-1} \text{ K}^{-2}$. A superconducting sample with $T_{\text{c}} = 0.68$ K shows a very well-defined specific heat jump at T_{c} , with $\Delta C/\gamma T_{\text{c}} = 1.31$. This is good evidence for bulk superconductivity, but further analysis was not pursued [21]. A more recent study of a $\text{Ba}_{0.6}\text{K}_{0.4}\text{Fe}_2\text{As}_2$ single crystal [22] found an ~ 1 K wide specific heat peak at $T_{\text{c}} = 34.6$ K and probed the field dependence of the feature. Evidence for strong coupling was found and the $\kappa = \lambda/\xi$ values were over 100.

There have been relatively few predictions made concerning the heat capacity of the pnictide superconductors, but one is particularly relevant to our work here [23]. It has been suggested that $\text{SmFeAsO}_{1-x}\text{F}_x$ has a nematic electronic phase overlapping the superconducting phase, probably in the doping range considered here. The low-temperature specific heat would change from $C \propto T^{\beta}$, $\beta < 2$ in the superconducting phase to $C \propto T^{2/3}$ in the nematic phase, with a crossover to the conventional $d = 3$ scalings $C \propto T$ close enough to the nematic critical point.

3. Experimental details

The $\text{SmFeAsO}_{1-x}\text{F}_x$ samples were synthesized by conventional solid state reaction methods, as described in [3, 4]. Standard powder x-ray diffraction patterns were measured, where all peaks could be indexed to the tetragonal ZrCuSiAs -type structure. Dc resistivity and

⁶ Recent work [13] has suggested that the nominal doping in $\text{SmFeAsO}_{1-x}\text{F}_x$ overestimates the F-doping by a factor of up to 2.5. Here we use the nominal doping to allow easy comparison of our samples with previous work carried out on them [3, 4, 24]. A comparison with the results in [12] suggests the correction factor suggested in [13] is approximately correct.

magnetization measurements were made to determine the midpoint (10–90% width) of the resistive and diamagnetic transitions with $T_c = 10(7)$, $17(8)$ and $25(8)$ K for $x = 0.1$, 0.12 and 0.13 , respectively. These samples have previously been investigated using μ SR [24], which suggested the coexistence of superconductivity and magnetism, with $T_N^{\text{Fe}} = 60$, 35 and 30 K, respectively. $\text{LaFeAsO}_{0.9}\text{F}_{0.1}$ ($T_c = 22$ K) was synthesized by a method adapted from [2]; a mixture of La, La_2O_3 , LaF_3 , Fe and As was heated at 600°C for 12 h in an evacuated silica ampoule, then thoroughly re-ground, pelletized and heated to 1150°C for a further 48 h in the evacuated silica. The resulting material was examined by laboratory-powder x-ray diffraction and found to contain $\text{LaFeAsO}_{0.9}\text{F}_{0.1}$ ($T_c = 22$ K) as the majority phase with small amounts of FeAs (<5 mol%) and LaOF (<2.5 mol%). The LiFeAs sample used in our experiments was synthesized by the method described in [8] and corresponds to sample 2 described in that study, with $T_c = 12$ K. While the diamagnetic shift in this sample is far smaller than the ideal, or that of the $T_c = 16$ K sample [8], μ SR measurements on this sample demonstrated that the superconducting sample volume was $>80\%$ [25], suggesting that particle size effects may be affecting the bulk dc susceptibility measurement.

The heat capacity measurements were carried out using a Quantum Design Physical Properties Measurement System (PPMS) over the temperature range 0.4 – 300 K; with measurements below 2 K were carried out using the standard ^3He insert. Samples were in the form of pressed powder pellets and were affixed to the measurement stage using Apiezon N-grease. The measurement technique employed by the PPMS is the two-tau relaxation method [26, 27], where the temperature of the sample is measured while a heat pulse is applied and for an equal time afterwards while the sample cools. The time dependence of the temperature variation in each part of the measurement is described by the sum of two exponentials describing the heat capacity of the sample and the measurement stage, and the coupling between them. The effectiveness of this technique is discussed critically by Lashley *et al* [28], and we can expect the absolute heat capacity values to be correct within $\pm 2\%$ for $5 \leq T \leq 300$ K and $\pm 5\%$ for $T \leq 5$ K. These errors are comparable with the error in the sample mass. For all compounds, we plot heat capacities per mole of formula unit.

4. ^4He results on oxypnictides

The data for the oxypnictide materials $\text{SmFeAsO}_{0.9}\text{F}_{0.1}$, $\text{SmFeAsO}_{0.88}\text{F}_{0.12}$, $\text{SmFeAsO}_{0.87}\text{F}_{0.13}$ and $\text{LaFeAsO}_{0.9}\text{F}_{0.1}$ from 2 to 200 K are shown in figure 1. The lattice and electronic parts of the heat capacity data are fitted to the equation:

$$C(T) = \gamma T + A_D C_D(T, \theta_D) + A_E C_E(T, \theta_E), \quad (1)$$

where γ is the Sommerfeld coefficient, and C_D and C_E are Debye and Einstein functions, respectively. We found that the data were well described by including only one Einstein mode, giving a more simple fitting function than was used by Tropeano *et al* [12]. The total amplitude of the lattice modes is close to that expected from the Dulong–Petit law. Fits were carried out over the temperature range $10 \leq T/\text{K} \leq 200$ K as Apiezon N grease produces small heat capacity anomalies above 200 K. The parameters derived from fitting equation (1) to the data shown in figure 1 are shown in table 1. As is apparent from figure 1, the lattice contributions are almost identical for the four samples, and the main differences are the change in the electronic term γ going from the La compound to the Sm compounds, and the λ anomalies at T_N^{Sm} (hereafter T_N) in each of the Sm samples. The difference between the γ values of the Sm and La

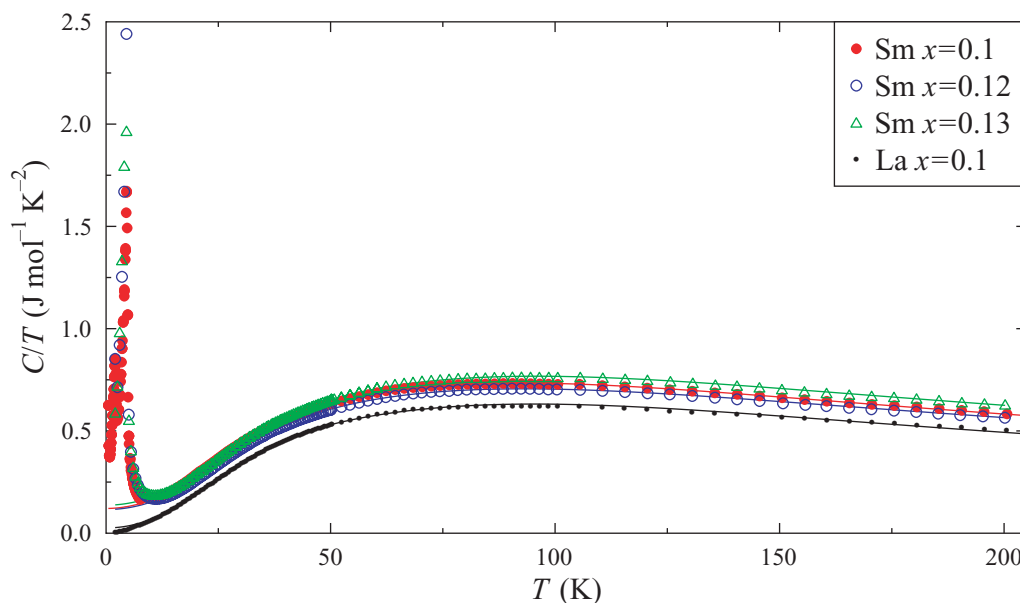


Figure 1. Raw heat capacity data on $\text{SmFeAsO}_{0.9}\text{F}_{0.1}$, $\text{SmFeAsO}_{0.88}\text{F}_{0.12}$, $\text{SmFeAsO}_{0.87}\text{F}_{0.13}$ and $\text{LaFeAsO}_{0.9}\text{F}_{0.1}$. The fits are described in the text and the parameters are shown in table 1.

Table 1. Lattice heat capacity fitting parameters derived from fitting equation (1) to the raw heat capacity data for the $\text{SmFeAsO}_{1-x}\text{F}_x$ and $\text{LaFeAsO}_{0.9}\text{F}_{0.1}$ samples described in section 4, and the LiFeAs sample described in section 6. The units for θ_D and θ_E are K, for A_D and A_E are $\text{J mol}^{-1} \text{K}^{-2}$, and for γ $\text{mJ mol}^{-1} \text{K}^{-2}$. Quoted errors are 1σ from the fitting.

Compound	θ_D	θ_E	A_D	A_E	γ
Sm ($x = 0.1$)	212(1)	380(3)	51(1)	59(1)	121(1)
Sm ($x = 0.12$)	227(2)	404(13)	55(1)	53(2)	116(1)
Sm ($x = 0.13$)	227(2)	407(8)	58(1)	61(1)	137(1)
La ($x = 0.1$)	212(1)	394(4)	51(1)	62(1)	26(7)
LiFeAs	194(2)	364(4)	24(1)	58(1)	23.3(5)

compounds, ~ 120 versus $26 \text{ mJ mol}^{-1} \text{K}^{-2}$, is quite remarkable. Our values of γ are comparable with those reported by Ding *et al* [11] for samples with slightly different dopings. Similarly, high values of γ have been observed in Nd (as we show in section 5) and Ce oxypnictides.

In figure 2, the raw data near T_N and the residues between the data in figure 1 and the fits given in table 1 near T_c are shown. The peak in C/T near T_N is clear for each of the samples and we can see the slow drop in T_N with increasing doping. Carrying out entropy subtractions suggested that the magnetic entropy was also dropping as the doping was increased and in the $x = 0.1$ and 0.12 samples an upturn in C/T was observed at the lowest temperatures; though we will see in section 5, this is a hint of what is actually going on at low temperatures.

Near the superconducting T_c and T_N^{Fe} in the right-hand panel of figure 2, the difference between the data and the fits is far smaller. It seems that the peak around T_c in the La compound

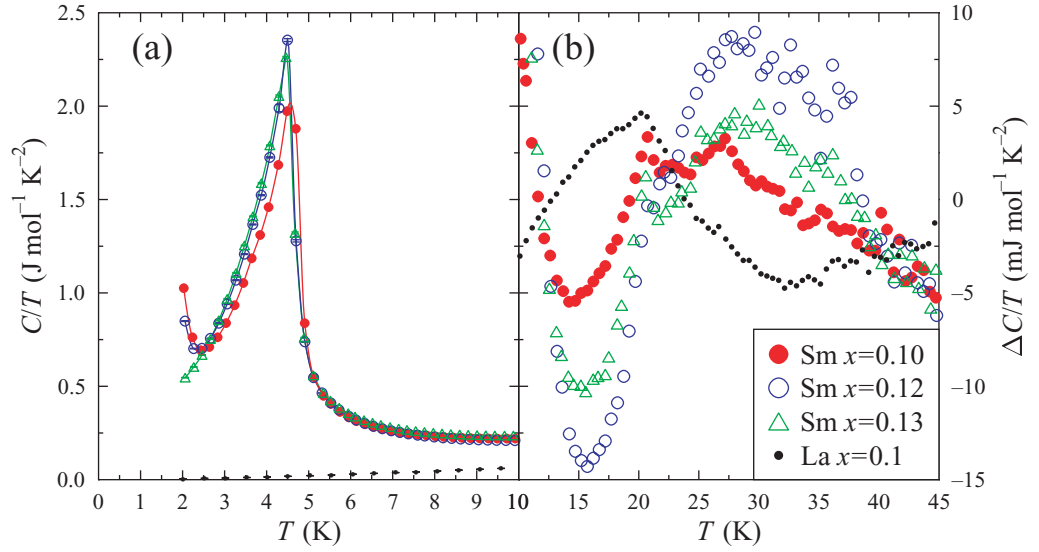


Figure 2. (a) C/T around T_N showing the shape of the peaks and the upturn at low temperatures, which we investigate further in section 5. (b) Difference between the data and the lattice + linear fit in the region of T_c for each of the samples. In $\text{LaFeAsO}_{0.9}\text{F}_{0.1}$ and $\text{SmFeAsO}_{0.9}\text{F}_{0.1}$, the peak can be identified with the superconducting transition, whereas in the other two $\text{SmFeAsO}_{1-x}\text{F}_x$ samples Fe magnetic ordering also contributes. Note the difference in vertical scale between panels (a) and (b).

is well defined and of a size similar to those found previously [17]. In the Sm compounds, the temperatures of T_c and T_N^{Fe} have been determined by other techniques [24]. The feature seems to grow with increasing doping and the $x = 0.1$ sample must correspond to the superconducting transition as the magnetic transition is at far higher temperature (and seems to be evident at ~ 50 K in figure 3). In the $x = 0.12$ sample, the anomaly starts at T_c and continues up to T_N^{Fe} . The $x = 0.13$ sample has almost coincident T_c and T_N^{Fe} and we observe a broad and less-structured feature at the appropriate temperature.

Seeing that the entropy values extracted from the low-temperature Néel ordering of the Sm magnetic moments approximate much more closely to $S = \frac{1}{2}$ [11, 12] than the $S = \frac{5}{2}$ expected for free ions [29], we sought to investigate the possibility of a Schottky-like anomaly due to the crystal field levels being gradually populated with increasing temperature. This can be done by comparing the heat capacity of Sm- and La-containing oxypnictides, but it would be challenging to attempt this on undoped samples since significant anomalies appear at the structural- and magnetic-phase transition(s) near 150 K. Instead, we used our measurements of the 10% doped samples where there are no superconducting and magnetic anomalies above 55 K. From the La compound, we get an excellent estimate of the lattice contribution because there is no rare-earth moment, and we can easily adjust for the difference in the Sommerfeld coefficient in our fitting of the difference. We took a direct molar subtraction between data sets measured at common temperature points and fitted the difference, $\Delta C = C(\text{Sm}) - C(\text{La})$ shown in figure 3, to the function:

$$\Delta C = \Delta\gamma T + R \left(\frac{Z_2}{Z_0} - \frac{Z_1}{Z_0} \right) \left(\frac{Z_1}{Z_0} \right), \quad (2)$$

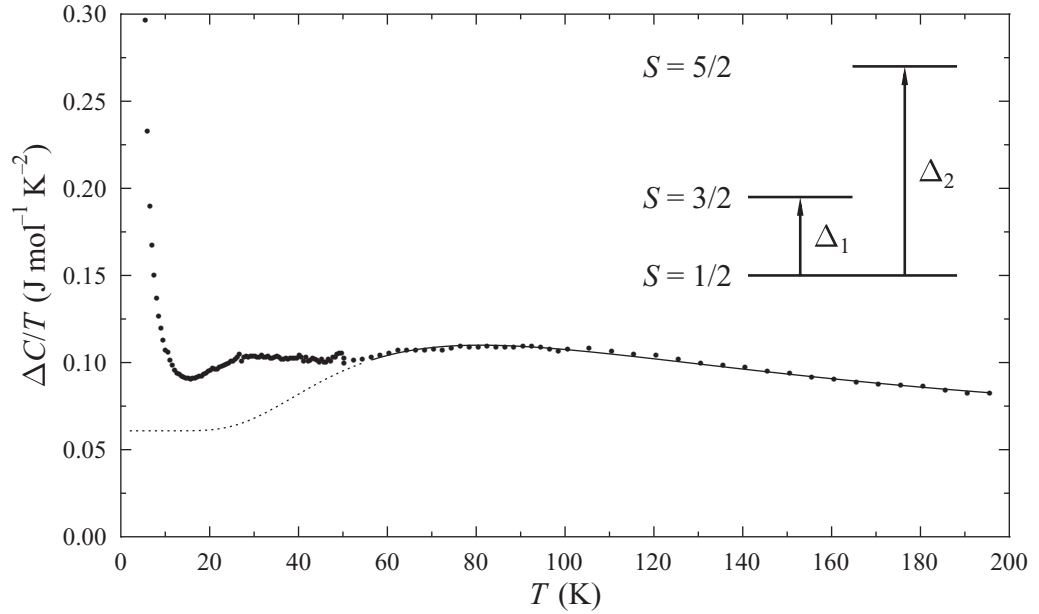


Figure 3. Difference $\Delta C/T$ between the molar heat capacities of $\text{SmFeAsO}_{0.9}\text{F}_{0.1}$ and $\text{LaFeAsO}_{0.9}\text{F}_{0.1}$ with a fit to equation (2). The solid line depicts the fitted region between 55 and 200 K, and the dashed line shows how this Schottky-like anomaly extends to low temperature. The inset shows the crystal field levels used to derive this model and the energy gaps between them.

$$Z_0 = g_1 \exp\left(-\frac{\Delta_1}{T}\right) + g_2 \exp\left(-\frac{\Delta_2}{T}\right), \quad (3)$$

$$Z_1 = \frac{g_1 \Delta_1}{T} \exp\left(-\frac{\Delta_1}{T}\right) + \frac{g_2 \Delta_2}{T} \exp\left(-\frac{\Delta_2}{T}\right), \quad (4)$$

$$Z_2 = \frac{g_1 \Delta_1^2}{T^2} \exp\left(-\frac{\Delta_1}{T}\right) + \frac{g_2 \Delta_2^2}{T^2} \exp\left(-\frac{\Delta_2}{T}\right), \quad (5)$$

where $\Delta\gamma$ is the difference between the electronic specific heats, g_i are the degeneracies of each of the levels and Δ_1 and Δ_2 are the energy gaps (in K) of the $S = \frac{1}{2} \rightarrow S = \frac{3}{2}$ and $S = \frac{1}{2} \rightarrow S = \frac{5}{2}$ transitions, respectively. (These are depicted in the inset of figure 3.) The parameters derived from this analysis are $\Delta_1 = 232(2) \text{ K} = 20.0(2) \text{ meV}$ and $\Delta_2 = 520(10) \text{ K} = 45(1) \text{ meV}$. The former value is in reasonable agreement with the estimates coming from the thermal activation of the μSR relaxation rate [30, 31] and the latter value has previously been derived from magnetic susceptibility measurements ($\Delta = 520 \text{ K}$ for $x = 0$ and $\Delta = 620 \text{ K}$ for $x = 0.15$) [29]. Sm containing materials are not amenable to investigation using inelastic neutron scattering, which is generally the most powerful probe of the crystal field levels in these materials. However, $\text{CeFeAsO}_{1-x}\text{F}_x$ has been investigated, and crystal field doublets at 0, 18.7 and 58.4 meV have been found for an $x = 0.16$ superconducting sample [32]. In the undoped sample, three doublets in the paramagnetic phase split into six singlets in the antiferromagnetic phase. It is interesting to note the similarity between the crystal field levels in these two materials and the observation that the 18.7 meV mode has a strongly enhanced local magnetic

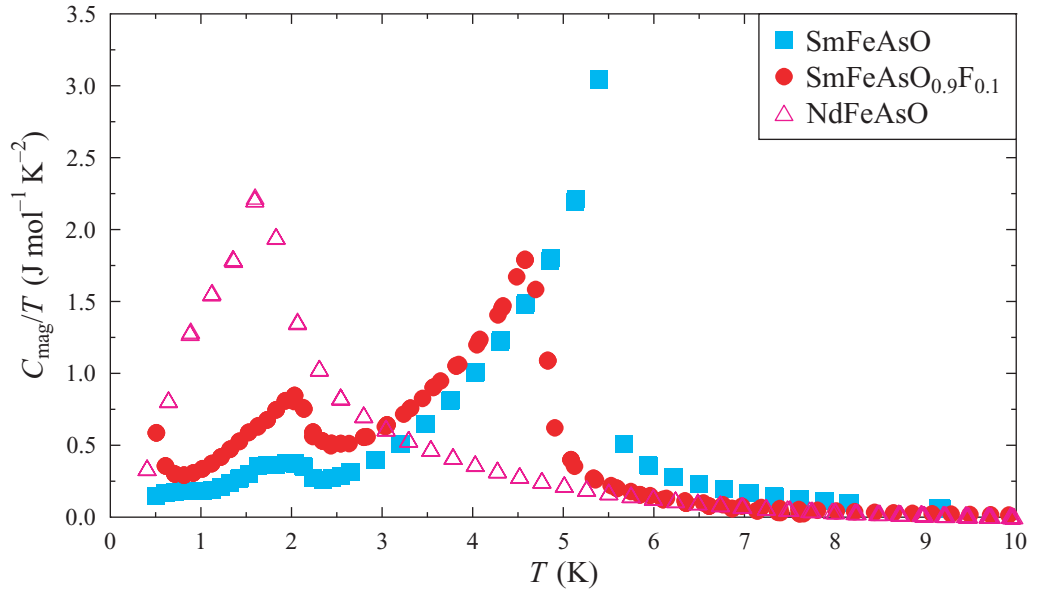


Figure 4. ^3He heat capacity data on SmFeAsO, NdFeAsO and SmFeAsO_{0.9}F_{0.1}. The subtraction of lattice terms to calculate C_{mag}/T is discussed in the text.

susceptibility below T_c , which is reminiscent of the increased μSR relaxation rates observed for the Sm compounds [30, 31]. The other parameter extracted from this analysis is the difference in the Sommerfeld coefficients, $\Delta\gamma = 60.8(3) \text{ mJ mol}^{-1} \text{ K}^{-2}$, which is far lower than the values extracted from fitting the raw data. This would suggest that the true value of $\gamma \sim 85 \text{ mJ mol}^{-1} \text{ K}^{-2}$ in the Sm oxypnictides—still significantly larger than for LaFeAs(O, F). (Ding *et al* [11] found a similar value from some of their fitting.) It seems likely that failing to include the Schottky-like anomaly due to the crystal field levels in the fitting of the raw data leads to an erroneously high value of γ , as we found above and has been noted by other reports [11]. Observing the doping dependence of the crystal field levels in these materials is likely to prove a fruitful area of future study, particularly, since the rare-earth moment fluctuations are evidently well coupled to the Fe fluctuations in the FeAs planes [30, 32].

5. ^3He results on oxypnictides

Our ^3He heat capacity results for SmFeAsO, SmFeAsO_{0.9}F_{0.1} and NdFeAsO are plotted in figure 4, after the subtraction of non-magnetic backgrounds. We made the assumption that the lattice contribution to the Sm samples would be identical and used the La lattice background for the Nd and corrected for the difference in the Sommerfeld coefficients, estimating a value for the Nd compound of $\sim 60 \text{ mJ mol}^{-1} \text{ K}^{-2}$. The Nd and Sm magnetic ordering lead to well-defined λ anomalies at the Néel temperature of the rare-earth moments. We find $T_N^{\text{Nd}} = 1.9 \text{ K}$ in reasonable agreement with the value determined by neutron diffraction ($T_N = 1.96(3) \text{ K}$ [33]). Other neutron diffraction measurements have shown that the Fe moments order at around 141 K with an ordered moment of $0.25(7)\mu_B$ [34]. We discuss the temperature variation of T_N^{Sm} with doping in section 7.

In the two Sm samples, we see a further anomaly below the previously determined T_N values at around 2 K. This feature grows significantly with increasing x as the feature at T_N

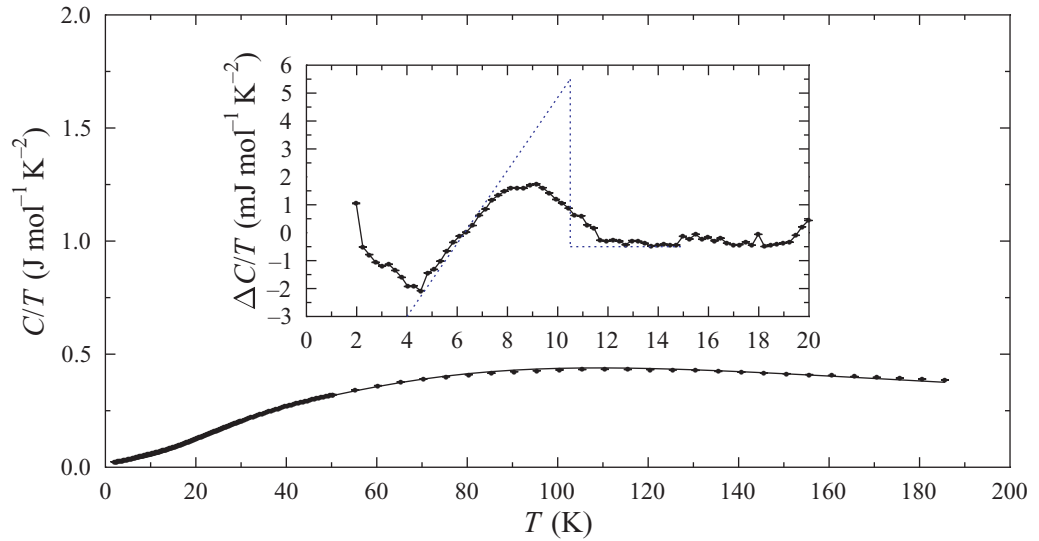


Figure 5. Heat capacity of LiFeAs with a fit to equation (1) above 10 K. The inset shows the difference between 0 and 12 T points, with a triangular approximation to the peak discussed in the text.

decreases in amplitude. We are unaware of any previous measurements on $\text{SmFeAsO}_{1-x}\text{F}_x$ below 2 K that have shown this feature, though our ^4He measurements show an upturn at low temperature (figure 2) that implies something must be occurring, and the decrease in the height at T_N has been reported elsewhere, if not discussed [11, 12]. We note that if the superconducting state is becoming more robust with increasing doping there will be a drop in the electronic contribution to the specific heat below T_c ($> T_N$). This would lead to a drop in the height of the magnetic features before the background is subtracted and a reduced estimate of the magnetic entropy after background subtraction.

6. LiFeAs

The LiFeAs sample ($T_c = 12$ K) gives us an opportunity to observe the superconducting behaviour without the effects of magnetic ordering of either rare-earth or iron moments. Since it superconducts without any significant non-stoichiometry, we compare our results with those on LaFePO reported elsewhere [18]–[20]. The lattice contribution to the heat capacity seems to be similar to that in the oxypnictides described in section 4 above, and we model it using equation (1) with the parameters shown in table 1. Data of LiFeAs in zero-field (with the fit to equation (1)) are shown in figure 5 and we plot the difference between the zero-field and 12 T data in the inset. A clear peak is found in the vicinity of T_c , although it is evidently broadened, as we would expect on the basis of susceptibility measurements [8]. (We also see a difference between the heat capacity traces above 20 K, which we cannot explain.) In the inset, we plot a linear trend following the low-temperature behaviour of the peak in the residue and extending up to the midpoint of the transition to estimate the size of the specific heat anomaly in this compound. This has two inherent difficulties: the transition is relatively broad and may affect the curvature below T_c to a greater extent than we have assumed, and more importantly, the upper critical field, B_{c2} , is far greater than our measurement field. On the basis of susceptibility

Table 2. Néel temperatures and magnetic entropy values for the samples investigated in this work. The methodology is discussed in sections 4 and 5. Entropies extracted for $\text{SmFeAsO}_{0.88}\text{F}_{0.12}$ and $\text{SmFeAsO}_{0.87}\text{F}_{0.13}$ are estimates due to the lack of ^3He data, calculated by assuming a smooth trend down to $T = 0$. The error bars are based on the quoted accuracy of the calorimeter at low temperatures [27, 28].

Doping (x)	T_N (K)	$S_{\text{mag}}/R \ln 2$
NdFeAsO	1.90(5)	0.96(10)
SmFeAsO	5.4(1)	0.91(10)
$\text{SmFeAsO}_{0.9}\text{F}_{0.1}$	4.65(5)	0.95(10)
$\text{SmFeAsO}_{0.88}\text{F}_{0.12}$	4.50(5)	~ 0.90
$\text{SmFeAsO}_{0.87}\text{F}_{0.13}$	4.45(5)	~ 0.67

measurements $B_{c2} > 80 \text{ T}$ [9], a result which is consistent with the value is extracted from μSR measurements [25]. T_c is therefore likely to have only been shifted by $< 1 \text{ K}$ by our measurement field and hence the residue does not have a full subtraction of the superconducting part of the heat capacity. From the line plotted in the inset, we can estimate the normalized specific heat jump at T_c to be $\Delta C/\gamma T_c = 0.26$, with $\gamma \sim 23 \text{ mJ mol}^{-1} \text{ K}^{-2}$. This is about $1/3$ the value found for LaFePO , which has a much lower $B_{c2} \sim 3.5 \text{ T}$ [20]. The small specific heat jump might suggest a small superconducting sample volume, which magnetic susceptibility measurements also suggested [8], but μSR measurements on a sample from the same batch gave a superconducting sample volume $> 80\%$ [25]. On this basis, the small shift in T_c is more likely to have led to the small specific heat jump. Both higher applied magnetic fields and samples with a more sharply defined T_c will be necessary to gain a more complete understanding of the thermodynamic properties of LiFeAs .

7. Discussion

Our results show a new feature in the heat capacity of $\text{SmFeAsO}_{1-x}\text{F}_x$ at around 2 K , which appears to grow and shift to lower temperature with increasing doping. We are not aware of this feature being reported elsewhere, nor any predictions of such a feature. Since the entropy released at the T_N peak seems to be dropping as this feature grows, it seems likely that this 2 K feature is related to the Sm moments. The presence of the feature at low temperature in the undoped sample suggests that it is not related to the nematic phase suggested by Xu *et al* [23] if their phase diagram is appropriate. Alternatives may be successive ordering of components of the Sm magnetic moments or reorientations of the moments between states with a different entropy, which are altered by the doping-dependent orthorhombic to tetragonal structural distortion [35]. In NdFeAsO , we have verified the T_N value previously determined using neutron scattering [33]. In table 2, we have collated the values of T_N determined in this study and the magnetic entropy values extracted. Our undoped Sm oxypnictide has a higher T_N than has been suggested by previous studies [11, 12]. It is not clear at this stage why this value is increased above previous measurements, although our value does sit closer to the trend of decreasing T_N with increasing doping suggested by other measurements. Where we have ^3He

data the magnetic entropy values are $R \ln 2$ within the experimental error (we take this to be the low-temperature accuracy of the cryostat) but for $\text{SmFeAsO}_{0.88}\text{F}_{0.12}$ and $\text{SmFeAsO}_{0.87}\text{F}_{0.13}$ the data above 2 K suggest that a significant amount of entropy is missing. Given the behaviour seen in the $\text{SmFeAsO}_{0.9}\text{F}_{0.1}$ sample, it seems very likely that a similar feature is present below 2 K and accounts for this missing entropy. The entropy values we obtain for the rare-earth moment ordering suggest that both Sm and Nd are in a $S = \frac{1}{2}$ state at low temperature. In the Sm $x = 0.1$ sample, we found that the higher temperature heat capacity includes a Schottky-like anomaly due to the higher crystal field levels at 20 and 45 meV above the ground state. These levels are similar to those observed for superconducting $\text{CeFeAsO}_{0.84}\text{F}_{0.16}$ using inelastic neutron scattering (0, 18.7 and 58.4 meV) [32]. It will be interesting to discover the variation of these crystal field levels in other materials as this field of research progresses, particularly if the rare-earth moments have any influence on the superconductivity.

The heat capacity features associated with the superconducting transitions in $\text{SmFeAsO}_{1-x}\text{F}_x$ are less well defined than those reported for superconducting samples without any magnetic transitions. The fit residues suggest that both magnetic and superconducting transitions contribute features, but while they are present at the temperatures suggested by other techniques [24], the entropy change is small and diffuse. The features in $\text{LaFeAsO}_{0.9}\text{F}_{0.1}$ and LiFeAs are better defined and are comparable with other reports on similar samples.

8. Conclusions

We have studied a series of Sm-, Nd- and La-containing oxypnictides and investigated the effect that the rare-earth magnetic moments have on the magnetism and superconductivity. The λ anomalies at each Néel temperature give clear evidence for ordering of the rare-earth moments, confirming previous studies. We have extended those studies by investigating the form of the heat capacity in the Sm samples below 2 K, which provides evidence for a new feature occurring slightly below 2 K that grows with increasing doping. This provides a natural explanation for the previously observed drop in the size of the peak at $T_N \sim 4$ K with increasing doping. We also probed the crystal field levels of the Sm^{3+} ions in $\text{SmFeAsO}_{0.9}\text{F}_{0.1}$ and found that they were consistent with both the $R \ln 2$ entropy associated with magnetic ordering at low temperature and also the free spin $S = \frac{5}{2}$ value observed at high temperature. The energies of the levels appear to be similar to those found in superconducting $\text{CeFeAsO}_{0.84}\text{F}_{0.16}$ using inelastic neutron scattering. In $\text{LaFeAsO}_{0.9}\text{F}_{0.1}$ and LiFeAs , we see distinct anomalies due to the superconducting transitions, whereas in the $\text{SmFeAsO}_{1-x}\text{F}_x$ samples, magnetic contributions complicate the form of the data and the superconducting contribution is less distinct. There remain many avenues to be explored using heat capacity in this fast moving field, including the possibility of nematic electronic order when superconductivity has been suppressed in $\text{SmFeAsO}_{1-x}\text{F}_x$, and the trends of crystal field levels as the rare-earth ions are substituted and the oxygen doping is changed; but it is already clear that this fundamental thermodynamic technique, coupled with careful analysis, can provide much useful information on the properties of FeAs-based compounds.

Acknowledgments

We are grateful to Christian Bernhard, Andrew Boothroyd, Alan Drew and Paul Goddard for their helpful discussions, and to Prabhakaran Dharmalingam for his experimental assistance. This work was supported by the EPSRC and STFC (UK).

References

- [1] Kamihara Y *et al* 2006 *J. Am. Chem. Soc.* **128** 10012
- [2] Kamihara Y *et al* 2008 *J. Am. Chem. Soc.* **130** 3296
- [3] Chen X H *et al* 2008 *Nature* **453** 761
- [4] Liu R H *et al* 2008 *Phys. Rev. Lett.* **101** 087001
- [5] Ren Z-A *et al* 2008 *Europhys. Lett.* **83** 17002
- [6] Rotter M *et al* 2008 *Phys. Rev. Lett.* **101** 107006
- [7] Sasmal K *et al* 2008 *Phys. Rev. Lett.* **101** 107007
- [8] Pitcher M J *et al* 2008 *Chem. Commun.* 5918
- [9] Tapp J H *et al* 2008 *Phys. Rev. B* **78** 060505
- [10] Parker D R *et al* 2008 arXiv:0810.3214
- [11] Ding L *et al* 2008 *Phys. Rev. B* **77** 180510
- [12] Tropeano M *et al* 2008 *Phys. Rev. B* **78** 094518
- [13] Hess C *et al* 2008 arXiv:0811.1601
- [14] McGuire M A *et al* 2008 *Phys. Rev. B* **78** 094517
- [15] Dong J *et al* 2008 *Europhys. Lett.* **83** 27006
- [16] McGuire M A *et al* 2009 *New J. Phys.* **11** 025011
- [17] Gang M *et al* 2008 *Chin. Phys. Lett.* **25** 2221
- [18] McQueen T M *et al* 2008 *Phys. Rev. B* **78** 024521
- [19] Kohama Y *et al* 2008 *J. Phys. Soc. Japan* **77** 094715
- [20] Analytis J G *et al* 2008 arXiv:0810.5368
- [21] Ronning F *et al* 2008 *J. Phys.: Condens. Matter* **20** 342203
- [22] Welp U *et al* 2008 arXiv:0810.1944
- [23] Xu C *et al* 2008 *Phys. Rev. B* **78** 134507
- [24] Drew A J *et al* 2008 arXiv:0807.4876
- [25] Pratt F L *et al* 2008 arXiv:0810.0973
- [26] Hwang J S *et al* 1997 *Rev. Sci. Instrum.* **68** 94
- [27] Physical Properties Measurement System: Heat Capacity Option User's Manual, 11th edn (San Diego, CA: Quantum Design) <http://www.qdusa.com>
- [28] Lashley J C *et al* 2003 *Cryogenics* **43** 369
- [29] Cimberle R *et al* 2008 arXiv:0807.1688
- [30] Drew A J *et al* 2008 *Phys. Rev. Lett.* **101** 097010
- [31] Khasanov R *et al* 2008 *Phys. Rev. B* **78** 092506
- [32] Chi S *et al* 2008 *Phys. Rev. Lett.* **101** 217002
- [33] Qiu Y *et al* 2008 *Phys. Rev. Lett.* **101** 257002
- [34] Chen Y *et al* 2008 *Phys. Rev. B* **78** 064515
- [35] Margadonna S *et al* 2009 *Phys. Rev. B* **79** 014503